

Numerical techniques for solving the quantum constraint equation of generic lattice-refined models in loop quantum cosmology

William Nelson and Mairi Sakellariadou

King's College London, Department of Physics, Strand WC2R 2LS, London, U.K.

To avoid instabilities in the continuum semi-classical limit of loop quantum cosmology models, refinement of the underlying lattice is necessary. The lattice refinement leads to new dynamical difference equations which, in general, do not have a uniform step-size, implying complications in their analysis and solutions. We propose a numerical method based on Taylor expansions, which can give us the necessary information to calculate the wave-function at any given lattice point. The method we propose can be applied in any lattice-refined model, while in addition the accuracy of the method can be estimated. Moreover, we confirm numerically the stability criterion which was earlier found following a von Neumann analysis. Finally, the ‘motion’ of the wave-function due to the underlying discreteness of the space-time is investigated, for both a constant lattice, as well as lattice refinement models.

PACS numbers: 04.60.Kz, 04.60.Pp, 98.80.Qc

I. INTRODUCTION

Loop quantum gravity [1] canonically quantises space-time via triads and holonomies of the Ashtekar connection. Whilst a full understanding of the theory has yet to be reached, symmetry reduced versions akin to the Wheeler-de Witt mini-superspace model have been successfully developed [2]. As a first approximation the quantised holonomies were taken to be shift operators *with a fixed magnitude*. This results in the quantised Hamiltonian constraint being a difference equation with a constant interval between points on the lattice. Whilst these models are reasonably successful in studying certain aspects of the quantum regime [2, 3], it has been shown that they lead to serious instabilities in the continuum, semi-classical limit [4, 5]. In the underlying loop quantum gravity theory, the contributions to the (discrete) Hamiltonian operator depend on the state which describes the universe. As the volume grows (the universe expands), the number of contributions increases. Thus, the Hamiltonian constraint operator is expected to create new vertices of a lattice state (in addition to changing their edge labels), which in loop quantum cosmology result in a refinement of the discrete lattice.

It has been recently shown how this lattice refinement effect can be modelled and how this approach eliminates the problematic instabilities in the continuum era [6]. Whilst the continuum limit of these lattice refining models can be taken, there is a complication in directly evolving two-dimensional wave-functions, such as those necessary to study Bianchi models or black hole interiors. The information needed to calculate the wave-function at a given lattice point is not provided by previous iterations. Recently, it has been demonstrated [7] that a simple local interpolation scheme can be used to approximate the necessary data points, allowing direct numerical evolution of such two-dimensional systems.

In this paper, we show how Taylor expansions can be used to perform this interpolation

with a well-defined and predicable accuracy. We first develop the scheme for the one-dimensional homogeneous, isotropic cosmological case, which has analytic solutions. We use this simple example to show that the accuracy of the system is well controlled. We then study the two-dimensional case of a Schwarzschild interior, which cannot be exactly solved (for a general lattice refinement scheme). As our interpolation system is based only on Taylor expansions, all we require is that the function used to model the lattice refinement be analytic. This allows us to look in detail at the effects of general lattice refinement models, beyond the simplest cases considered thus far. We also examine the instability found in Ref. [5] and show numerically that the analytic conditions for stability found for a specific lattice refinement model, are indeed valid. We then look at how these conditions change with different lattice refinement models. Finally, we comment of the fact that the discrete nature of the underlying lattice introduces a *twist* into otherwise straight Gaussian wave-packets and explain its origin.

II. ELEMENTS OF LOOP QUANTUM COSMOLOGY

Loop quantum cosmology is not formulated in terms of metrics and coordinates, rather SU(2) holonomies of the connection, \hat{h}_k , and triads, \hat{p} , are used. In this set up the gravitational part of the Hamiltonian constraint¹, assuming flat homogeneous and isotropic models, reads [8]

$$\hat{C}_{\text{grav}}|\Psi\rangle = \frac{2i}{\kappa^2\hbar\gamma^3\tilde{\mu}^3}\text{tr}\sum_{ijk}\epsilon^{ijk}\left(\hat{h}_k\left[\hat{h}_k^{-1},\hat{V}\right]\hat{h}_i\hat{h}_j\hat{h}_i^{-1}\hat{h}_j^{-1}\right)|\Psi\rangle, \quad (2.1)$$

where $\kappa = 8\pi G$ and $\hat{V} = \widehat{|p|^{3/2}}$ is the volume operator. We use the irreducible representation, $J = 1/2$, so that the Hamiltonian constraint is not plagued of ill-behaving spurious solutions [9]. The action of the volume operator \hat{V} on the basis states $|\mu\rangle$ is given by

$$\hat{V}|\mu\rangle = \widehat{|p|^{3/2}}|\mu\rangle = \left(\frac{\kappa\gamma\hbar|\mu|}{6}\right)^{3/2}|\mu\rangle. \quad (2.2)$$

The basis states $|\mu\rangle$ are eigenstates of the triad, and eigenstates of the volume operator, with eigenvalues μ . They satisfy the orthonormality relation

$$\langle\mu_1|\mu_2\rangle = \delta_{\mu_1,\mu_2}. \quad (2.3)$$

The holonomy h_i (more precisely $h_i^{(\tilde{\mu})}$) is along the edge parallel to the $i^{(\text{th})}$ basis vector, whose length is set by $\tilde{\mu}$. The parameter γ is the Barbero-Immirzi parameter, a constant ambiguity parameter that can be fixed by considering black-hole entropy calculations [10, 11]. Classically, $p = a^2$, where a is the usual cosmological scale factor.

¹ The reader should note that the factor ordering we are using is not the *conventional* one. We make this choice because the Hamiltonian constraint for a lattice refinement model of the form $\tilde{\mu} = \mu_0\mu^{-A}$ with general A , turns out to be of the same form as that for the fixed lattice case. This simplifies the demonstration of our numerical method to solve the quantum evolution equation of generic lattice-refined models. Certainly, the validity of our method is independent of the choice for the factor ordering.

A general state $|\Psi\rangle$ in the kinematical Hilbert space can be expanded as

$$|\Psi\rangle = \sum_{\mu} \Psi_{\mu} |\mu\rangle , \quad (2.4)$$

with the requirement

$$\sum_{\mu} \bar{\Psi}_{\mu} \Psi_{\mu} < \infty , \quad (2.5)$$

so that the state has a finite kinematical norm.

The action of the holonomies of the Ashtekar connection on the basis states reads [8]

$$\hat{h}_i |\mu\rangle = (\widehat{\text{cs}}\mathbb{1} - i\sigma_i \widehat{\text{sn}}) |\mu\rangle , \quad (2.6)$$

where $\mathbb{1}$ is the identity 2×2 matrix, σ_i are the Pauli spin matrices and $\widehat{\text{cs}}$, $\widehat{\text{sn}}$ are given by

$$\begin{aligned} \widehat{\text{cs}}|\mu\rangle &\equiv \frac{1}{2} \left(\widehat{e^{i\tilde{\mu}\bar{c}/2}} + \widehat{e^{-i\tilde{\mu}\bar{c}/2}} \right) |\mu\rangle = \frac{1}{2} (|\mu + \tilde{\mu}\rangle + |\mu - \tilde{\mu}\rangle) \\ \widehat{\text{sn}}|\mu\rangle &\equiv \frac{1}{2} \left(\widehat{e^{i\tilde{\mu}\bar{c}/2}} - \widehat{e^{-i\tilde{\mu}\bar{c}/2}} \right) |\mu\rangle = \frac{1}{2i} (|\mu + \tilde{\mu}\rangle - |\mu - \tilde{\mu}\rangle) , \end{aligned} \quad (2.7)$$

with $\tilde{\mu}$ a real number.

The generalised isotropic connection $|\bar{c}\rangle$ is defined such that,

$$\langle \bar{c} | \mu \rangle = e^{i\mu\bar{c}/2} . \quad (2.8)$$

Using Eq. (2.7), the gravitational part of the Hamiltonian constraint, Eq. (2.1), can be written in the form of a difference equation

$$\hat{\mathcal{C}}_{\text{grav}} |\Psi\rangle = \frac{3}{2\kappa^2 \hbar \gamma^3 \tilde{\mu}^2} \sum_{\mu} S(\mu) [\Psi_{\mu+4\tilde{\mu}} - 2\Psi_{\mu} + \Psi_{\mu-4\tilde{\mu}}] |\mu\rangle , \quad (2.9)$$

where

$$\begin{aligned} S(\mu) &\equiv \frac{2}{\gamma \kappa \hbar \tilde{\mu}} |V_{\mu+\tilde{\mu}} - V_{\mu-\tilde{\mu}}| . \\ &= \frac{1}{3\tilde{\mu}} \sqrt{\frac{\kappa \gamma \hbar}{6}} \left| |\mu + \tilde{\mu}|^{3/2} - |\mu - \tilde{\mu}|^{3/2} \right| . \end{aligned} \quad (2.10)$$

From now on we set, for simplicity, $1/(2\sqrt{6\kappa^3 \hbar \gamma^5}) = 1$, so that the gravitational part of the Hamiltonian, Eq. (2.9) is,

$$\hat{\mathcal{C}}_{\text{grav}} |\Psi\rangle = \sum_{\mu} \frac{1}{\tilde{\mu}^3} \left| |\mu + \tilde{\mu}|^{3/2} - |\mu - \tilde{\mu}|^{3/2} \right| [\Psi_{\mu+4\tilde{\mu}} - 2\Psi_{\mu} + \Psi_{\mu-4\tilde{\mu}}] |\mu\rangle , \quad (2.11)$$

and the full Hamiltonian constraint reads

$$\left(\hat{\mathcal{C}}_{\text{grav}} + \hat{\mathcal{H}}_{\phi} \right) |\Psi\rangle = 0 , \quad (2.12)$$

where $\hat{\mathcal{H}}_\phi$ is the matter Hamiltonian, assumed to operate diagonally on the basis states, i.e., $\hat{\mathcal{H}}_\phi|\mu\rangle = \mathcal{H}_\phi|\mu\rangle$. Using Eq. (2.11), the full Hamiltonian constraint, Eq. (2.12), reads

$$\frac{1}{\tilde{\mu}^3} \left| |\mu + \tilde{\mu}|^{3/2} - |\mu - \tilde{\mu}|^{3/2} \right| [\Psi_{\mu+4\tilde{\mu}} - 2\Psi_\mu + \Psi_{\mu-4\tilde{\mu}}] = -\mathcal{H}_\phi, \quad (2.13)$$

Until recently, the magnitude of the shift operator, $\tilde{\mu}$, was taken to be a constant. This gave the resulting difference equation a fixed step-size making its analysis much simpler. However, in the full theory one expects that $\tilde{\mu}$ will be a decreasing function of μ and hence the step-size in the difference equation, Eq. (2.13), will vary. In essence, the difference equation is defined on a *refining lattice*. It has been shown that modelling of this lattice refinement is crucial for the stability of the classical cosmological wave-function [5, 6, 12].

In the case of an one-dimensional system, such as the one under consideration here, the problem can be mapped onto a fixed lattice simply by a change of basis. This depends somewhat on the precise form of lattice refinement, however all that is required for it to be possible is that the integral $\int \tilde{\mu}(\mu) d\mu$ exists. To be explicit, consider a lattice refinement model of the form

$$\tilde{\mu} = \mu_0 \mu^{-A},$$

where μ_0 is some constant [6]. If we then make the change of variables

$$\mu \rightarrow \nu = k \frac{\mu^{1-A}}{\mu_0(1-A)},$$

where k is a constant, equal to the magnitude of the shift operator associated with these new coordinates, Eq. (2.13) becomes

$$\frac{1}{k^3} S(\nu) [\Psi_{\nu+4k} - 2\Psi_\nu + \Psi_{\nu-4k}] = -\mathcal{H}_\phi, \quad (2.14)$$

where

$$|\Psi\rangle = \sum_\nu \psi_\nu |\nu\rangle, \quad (2.15)$$

and

$$S(\nu) = \left| |(\nu+k)\alpha|^{3/2/(1-A)} - |(\nu-k)\alpha|^{3/2/(1-A)} \right|, \quad (2.16)$$

with α defined as

$$\alpha \equiv \frac{\mu_0(1-A)}{k}.$$

The fact that the difference equations, Eq. (2.13) and Eq. (2.14), are of the same form is due to the choice of factor ordering. This allows us to directly compare numerical solutions of the two systems, since they will have the same large-scale limit. This is indeed the reason for our choice of factor ordering in Eq. (2.1).

Note that usually one wishes to use a self-adjoint Hamiltonian, however for simplicity (and to allow for a more direct comparison with the case of a black hole interior), we use the form given in Eq. (2.9), which is not self-adjoint. Certainly, the numerical method described below is also valid for the self-adjoint case, as well as for different factor orderings.

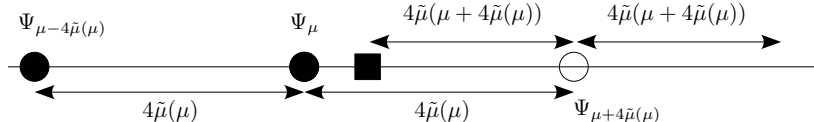


FIG. 1: This figure demonstrates the problem of evolving a difference equation that has been defined on a varying lattice. Given the value of Ψ defined on two adjacent lattice points (solid circles) one can use the difference equation to evaluate Ψ on the subsequent lattice site (open circle). However when one attempts to evaluate Ψ at the next lattice point, one finds that one does not have the necessary data point (square).

III. NUMERICAL EVOLUTION OF THE DIFFERENCE EQUATION

A. One-dimensional case

In the previous section we have seen how to transform the Hamiltonian constraint from an one-dimensional difference equation defined on a varying lattice, Eq. (2.13), to one on a constant lattice, Eq. (2.14). Thus, given the initial values of Ψ on two adjacent lattice points, one can iterate Eq. (2.14) to calculate Ψ on all lattice points. However, this mapping of the problem onto a constant lattice is not, in general, possible in two dimensions; one needs to develop a system that allows the use of the difference equation defined on the varying lattice, Eq. (2.13). It is clear that, given two values of Ψ defined on two adjacent lattice points, one can no longer iterate the difference equation to arbitrary μ [7] (see Fig. 1 which illustrates this problem). Assuming that the wave-function is *pre-classical* [13], i.e., that it varies slowly on scales smaller than the discreteness scale, one can use a Taylor expansion about previously calculated lattice sites to approximate the data necessary for the next iteration. This is equivalent to the local interpolation method used in Ref. [7]. The main advantage however of the Taylor expansion method we propose here is that it allows one to estimate the order of the approximation and, if necessary, increase the accuracy.

Being more explicit, consider the scheme depicted in Fig. 1, and set

$$\Psi_{\mu-4\tilde{\mu}(\mu)} = \Psi_1, \quad \Psi_\mu = \Psi_2, \quad \Psi_{\mu+4\tilde{\mu}(\mu)} = \Psi_3.$$

Given the value of Ψ_1 and Ψ_2 , one can use Eq. (2.13) to evaluate Ψ_3 . We then move to the next lattice point, so that $\bar{\Psi}_2 = \Psi_3$, where the over-line indicates this is the ‘new’ value. To calculate $\bar{\Psi}_1$ we make a Taylor expansion about Ψ_2 to get

$$\begin{aligned} \bar{\Psi}_1 = & \Psi_2 + \frac{1}{2} [\Psi_3 - 2\Psi_2 + \Psi_1] [1 - \Delta(\mu)] \\ & + \mathcal{O} \left[[\tilde{\mu}(\mu)]^2 [1 - \Delta(\mu)] \frac{d^2\Psi}{d\mu^2} \Big|_\mu \right] + \mathcal{O} \left[[\tilde{\mu}(\mu)]^2 \frac{d^3\Psi}{d\mu^3} \Big|_\mu \right], \end{aligned} \quad (3.1)$$

where

$$\Delta(\mu) = \frac{\tilde{\mu}(\mu_1)}{\tilde{\mu}(\mu)}, \quad \text{with } \mu_1 = \mu + 4\tilde{\mu}(\mu). \quad (3.2)$$

Here, we have only used the first-order terms in the expansion to calculate the required data point, with the second-order terms being used to keep track of the accuracy of the

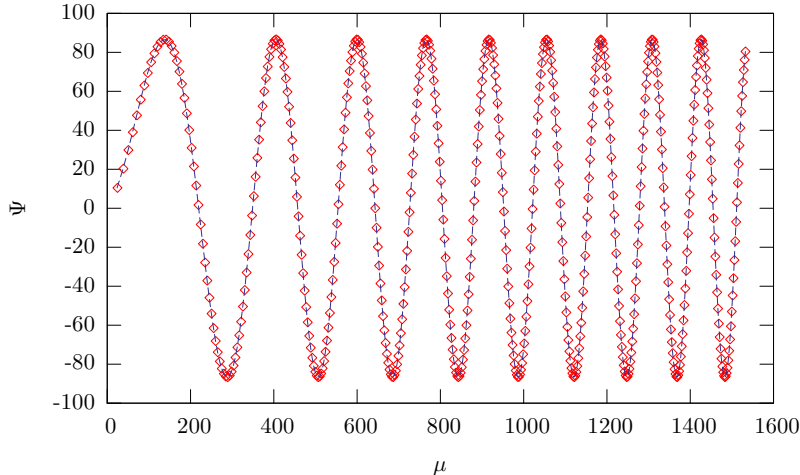


FIG. 2: The evolution of a wave-function using the Taylor expansion scheme. The circles are the approximated values calculated on the varying lattice, whilst the line is the exact wave-function. We use $\mu_0 = 1.0$, $A = -0.5$, $\mathcal{H}_\phi = 1.0 \times 10^{-4}$, $\mu_{\text{initial}} = 1.0$, and initial conditions $\Psi_1 = 0.0$, $\Psi_2 = 0.5$.

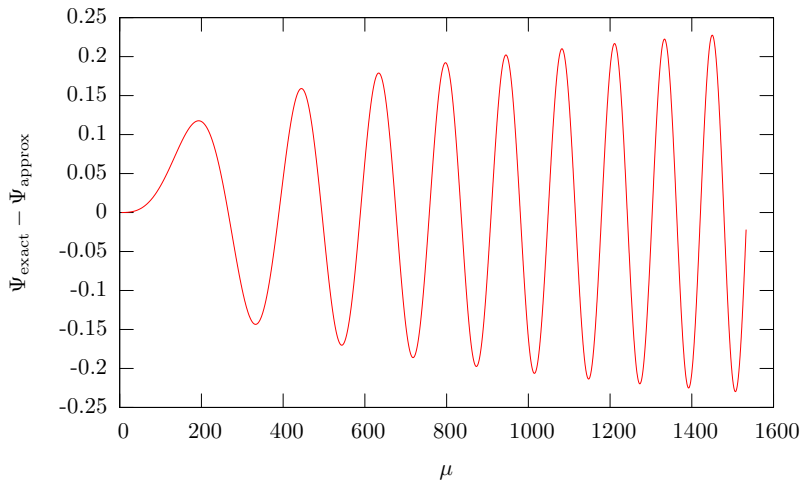


FIG. 3: The difference between the exact approximate wave-functions is less than one percent. This error is almost entirely due to the slight difference in the initial conditions between the two grids, i.e., the difference between the initial separation of Ψ_1 and Ψ_2 . We use $\mu_0 = 1.0$, $A = -0.5$, $\mathcal{H}_\phi = 1.0 \times 10^{-4}$, $\mu_{\text{initial}} = 1.0$, and initial conditions $\Psi_1 = 0.0$, $\Psi_2 = 0.5$.

approximation. This system readily extends to higher order. It should be noted that if higher order terms are required, then Eq. (2.13) must be used to evaluate terms like $\Psi_{\mu+8\tilde{\mu}(\mu)}$, $\Psi_{\mu+12\tilde{\mu}(\mu)}$, etc., so that the higher derivatives can be calculated.

As an example, we evaluate the wave-function using both, the exact case, Eq. (2.14), and Taylor expansion method described above. A small, constant matter Hamiltonian is used ($\mathcal{H}_\phi = 1.0 \times 10^{-4}$), to give the wave-functions some fine detail, however it should be remembered that there is now the possibility that gravitational back reaction may become

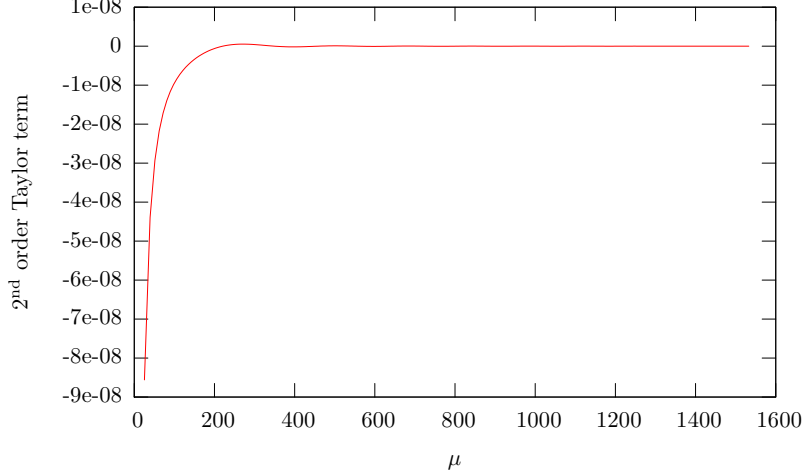


FIG. 4: The value of the next order term in the Taylor expansion. We use $\mu_0 = 1.0$, $A = -0.5$, $\mathcal{H}_\phi = 1.0 \times 10^{-4}$, $\mu_{\text{initial}} = 1.0$, and initial conditions $\Psi_1 = 0.0$, $\Psi_2 = 0.5$.

important. The resulting wave-functions, obtained with both approaches, are given in Fig. 2; their difference is plotted in Fig. 3. The next order term in the Taylor expansion is shown in Fig. 4. It is clear that, even at linear order, the Taylor expansion method is extremely accurate. The difference between the two wave-functions is almost entirely due to the fact that the separation between the two initial lattice points is not exactly the same, as a result of the lattice refinement of the $\tilde{\mu}(\mu)$ scheme. This alters the initial conditions slightly, nevertheless the discrepancy is still less than one percent.

It should be noted that if the lattice is not refining fast enough to ensure that the wave-function remains *pre-classical*, the interpolation method would begin to fail [6]. However, this would correspond to an unstable wave-function which would not have a classical large-scale limit.

B. Two-dimensional case

The cosmological quantisation procedure used in Section II can be adapted to the anisotropic geometry of a black hole interior. The resulting two-dimensional Hamiltonian constraint is again a difference equation defined on a varying lattice [5],

$$\begin{aligned}
& C_+(\mu, \tau) [\Psi_{\mu+2\delta_\mu, \tau+2\delta_\tau} - \Psi_{\mu-2\delta_\mu, \tau+2\delta_\tau}] \\
& + C_0(\mu, \tau) [(\mu + 2\delta_\mu) \Psi_{\mu+4\delta_\mu, \tau} - 2(1 + 2\gamma^2\delta_\mu^2) \mu \Psi_{\mu, \tau} + (\mu - 2\delta_\mu) \Psi_{\mu-4\delta_\mu, \tau}] \\
& + C_-(\mu, \tau) [\Psi_{\mu-2\delta_\mu, \tau-2\delta_\tau} - \Psi_{\mu+2\delta_\mu, \tau-2\delta_\tau}] = \frac{\delta_\tau \delta_\mu^2}{\delta^3} \mathcal{H}_\phi \Psi_{\mu, \tau} ,
\end{aligned} \tag{3.3}$$

with

$$C_\pm \equiv 2\delta_\mu \left(\sqrt{|\tau \pm 2\delta_\tau|} + \sqrt{|\tau|} \right) , \tag{3.4}$$

$$C_0 \equiv \sqrt{|\tau + \delta_\tau|} - \sqrt{|\tau - \delta_\tau|} , \tag{3.5}$$

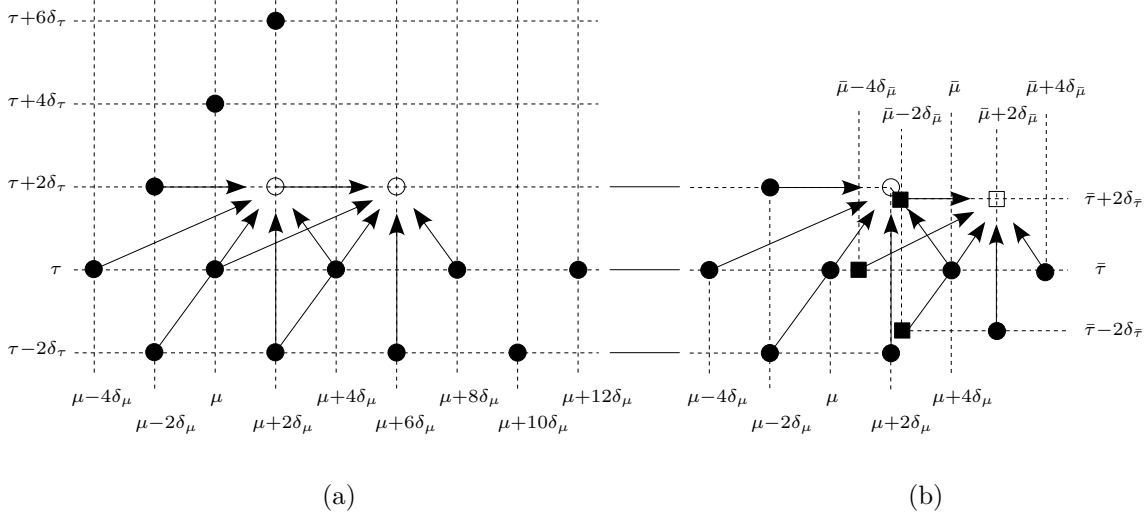


FIG. 5: (a) For the fixed lattice case the two-dimensional wave-function can be calculated, given suitable initial conditions (solid circles). (b) In the case of a refining lattice, the data needed to calculate the value of the wave-function at a particular lattice site (open square) is not given by previous iterations (solid squares). This is due to the fact that $\delta_\mu(\mu_i, \tau_i) - \delta_\mu(\mu_{i+1}, \tau_i) \neq 0$, where $\mu_{i+1} = \mu_i + 4\delta_\mu(\mu_i, \tau_i)$. To improve the clarity of the diagram, the explicit μ and τ dependence of the step-sizes is suppressed, and the notation $\delta_{\bar{\mu}} \equiv \delta_\mu(\mu_{i+1}, \tau_i)$, and $\delta_{\bar{\tau}} \equiv \delta_\tau(\mu_{i+1}, \tau_i)$ is used.

where we have defined δ_μ and δ_τ as the step-sizes along the μ and τ directions, respectively. The parameter δ , with $0 < \delta < 1$, gives the fraction of a lattice edge that the underlying graph changing Hamiltonian uses [5]. For clarity, the μ and τ dependence in $\delta_\mu(\mu, \tau)$ and $\delta_\tau(\mu, \tau)$ have been suppressed. The lattice spans the (μ, τ) -plane and since μ and τ are the coordinate lengths along the polar and radial coordinates, respectively, the (μ, τ) -plane corresponds to the (Θ, r) -plane of the black-hole interior.

Note that we have again assumed that the matter Hamiltonian acts diagonally on the basis states of the wave-function, namely

$$\hat{\mathcal{H}}_\phi |\Psi\rangle \equiv \hat{\mathcal{H}}_\phi \sum_{\mu, \tau} \Psi_{\mu, \tau} |\mu, \tau\rangle = \sum_{\mu, \tau} \mathcal{H}_\phi \Psi_{\mu, \tau} |\mu, \tau\rangle. \quad (3.6)$$

If δ_μ and δ_τ were constant, then Eq. (3.3) could be used to iteratively calculate the value of Ψ at each successive lattice point, given suitable initial conditions (see, Fig. 5a). If instead the lattice is refining, i.e., if δ_μ and δ_τ are decreasing functions of μ and τ , respectively, then we have the same problem as in the one-dimensional case (see, Fig. 5b). As in the one-dimensional case, one can use Taylor expansions to calculate the necessary data points. In general, given a function evaluated at three (non-co-linear) coordinates, the Taylor approximation to the value at a fourth position is given by

$$f(x_4, y_4) = f(x_2, y_2) + \delta_{42}^x \frac{\partial f}{\partial x} \Big|_{x_2, y_2} + \delta_{42}^y \frac{\partial f}{\partial y} \Big|_{x_2, y_2} + \mathcal{O}\left(\left(\delta_{42}^x\right)^2 \frac{\partial^2 f}{\partial x^2} \Big|_{x_2, y_2}\right) + \mathcal{O}\left(\left(\delta_{42}^y\right)^2 \frac{\partial^2 f}{\partial y^2} \Big|_{x_2, y_2}\right), \quad (3.7)$$

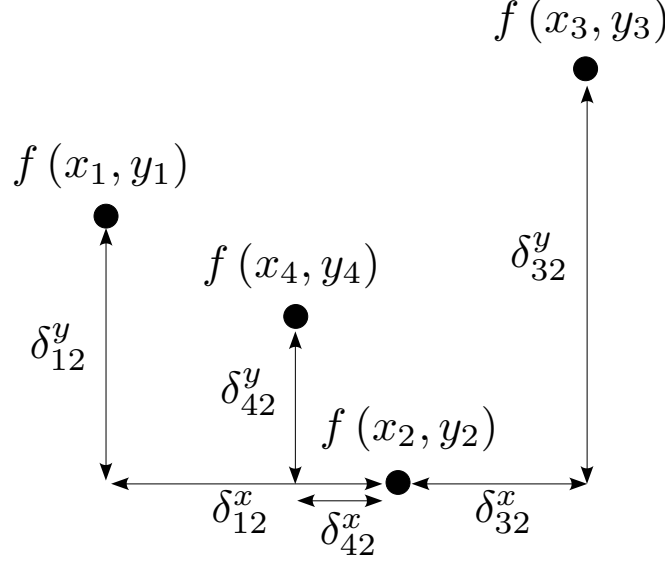


FIG. 6: Given the value of a function evaluated at three positions, (x_1, y_1) , (x_2, y_2) and (x_3, y_3) , a Taylor expansion can be used to approximate the value at a fourth point, (x_4, y_4) .

where the Taylor expansion is taken about the position (x_2, y_2) and we have defined $\delta_{ij}^x \equiv x_i - x_j$ and $\delta_{ij}^y \equiv y_i - y_j$ (see, Fig. 6). To approximate the differentials in Eq. (3.7), use points (x_1, y_1) and (x_3, y_3) :

$$f(x_1, y_1) = f(x_2, y_2) + \delta_{12}^x \frac{\partial f}{\partial x} \Big|_{x_2, y_2} + \delta_{12}^y \frac{\partial f}{\partial y} \Big|_{x_2, y_2} + \dots, \quad (3.8)$$

$$f(x_3, y_3) = f(x_2, y_2) + \delta_{32}^x \frac{\partial f}{\partial x} \Big|_{x_2, y_2} + \delta_{32}^y \frac{\partial f}{\partial y} \Big|_{x_2, y_2} + \dots, \quad (3.9)$$

where the dots indicate higher order terms. Solving for $\partial_x f$ and $\partial_y f$, gives

$$\begin{aligned} \frac{\partial f}{\partial x} \Big|_{x_2, y_2} &= \frac{\delta_{12}^y}{\Delta} [f(x_3, y_3) - f(x_2, y_2)] - \frac{\delta_{32}^y}{\Delta} [f(x_1, y_1) - f(x_2, y_2)] + \dots, \\ \frac{\partial f}{\partial y} \Big|_{x_2, y_2} &= \frac{\delta_{32}^x}{\Delta} [f(x_1, y_1) - f(x_2, y_2)] - \frac{\delta_{12}^x}{\Delta} [f(x_3, y_3) - f(x_2, y_2)] + \dots, \end{aligned}$$

where $\Delta \equiv \delta_{32}^x \delta_{12}^y - \delta_{32}^y \delta_{12}^x$.

As in the one-dimensional case, higher-order terms in the Taylor expansion can be used to improve the accuracy of the system. Here we calculate the second-order expansion to demonstrate that linear interpolation is sufficient for many interesting cases. Given five points $\Psi_1, \Psi_2, \Psi_3, \Psi_4$ and Ψ_5 , where $\Psi_n = \Psi(\mu_n, \tau_n)$, the second-order Taylor approximation for the sixth point, Ψ_6 , reads

$$\Psi_6 = \Psi_1 + \delta_{61}^\mu \frac{\partial \Psi}{\partial \mu} \Big|_1 + \delta_{61}^\tau \frac{\partial \Psi}{\partial \tau} \Big|_1 + \frac{(\delta_{61}^\mu)^2}{2} \frac{\partial^2 \Psi}{\partial \mu^2} \Big|_1 + \frac{(\delta_{61}^\tau)^2}{2} \frac{\partial^2 \Psi}{\partial \tau^2} \Big|_1 + \dots, \quad (3.10)$$

where as before $\delta_{ij}^\mu \equiv \mu_i - \mu_j$ and $\delta_{ij}^\tau \equiv \tau_i - \tau_j$; the derivatives are all evaluated at the point

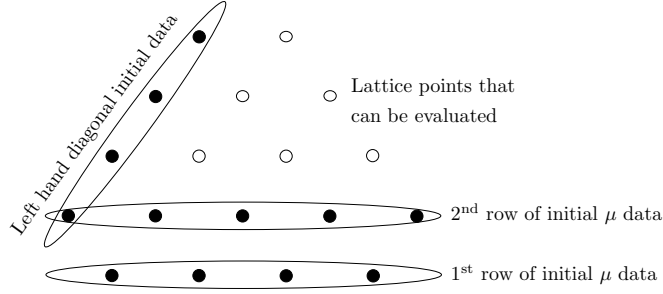


FIG. 7: The initial data (solid circles) is given on two adjacent μ rows and the lattice points along the left-hand (small τ) diagonal. This allows us to evaluate the wave-function on lattice points (open circles) within a triangular region of base $\mu_{\max} - \mu_{\text{initial}}$ and height $\tau_{\max} - \tau_{\text{initial}}$.

(μ_1, τ_1) . We can calculate the derivatives to the necessary order by solving the following system of simultaneous equations:

$$\begin{aligned}
\Psi_2 &= \Psi_1 + \delta_{21}^\mu \frac{\partial \Psi}{\partial \mu} \Big|_1 + \delta_{21}^\tau \frac{\partial \Psi}{\partial \tau} \Big|_1 + \frac{(\delta_{21}^\mu)^2}{2} \frac{\partial^2 \Psi}{\partial \mu^2} \Big|_1 + \frac{(\delta_{21}^\tau)^2}{2} \frac{\partial^2 \Psi}{\partial \tau^2} \Big|_1, \\
\Psi_3 &= \Psi_1 + \delta_{31}^\mu \frac{\partial \Psi}{\partial \mu} \Big|_1 + \delta_{31}^\tau \frac{\partial \Psi}{\partial \tau} \Big|_1 + \frac{(\delta_{31}^\mu)^2}{2} \frac{\partial^2 \Psi}{\partial \mu^2} \Big|_1 + \frac{(\delta_{31}^\tau)^2}{2} \frac{\partial^2 \Psi}{\partial \tau^2} \Big|_1, \\
\Psi_4 &= \Psi_1 + \delta_{41}^\mu \frac{\partial \Psi}{\partial \mu} \Big|_1 + \delta_{41}^\tau \frac{\partial \Psi}{\partial \tau} \Big|_1 + \frac{(\delta_{41}^\mu)^2}{2} \frac{\partial^2 \Psi}{\partial \mu^2} \Big|_1 + \frac{(\delta_{41}^\tau)^2}{2} \frac{\partial^2 \Psi}{\partial \tau^2} \Big|_1, \\
\Psi_5 &= \Psi_1 + \delta_{51}^\mu \frac{\partial \Psi}{\partial \mu} \Big|_1 + \delta_{51}^\tau \frac{\partial \Psi}{\partial \tau} \Big|_1 + \frac{(\delta_{51}^\mu)^2}{2} \frac{\partial^2 \Psi}{\partial \mu^2} \Big|_1 + \frac{(\delta_{51}^\tau)^2}{2} \frac{\partial^2 \Psi}{\partial \tau^2} \Big|_1.
\end{aligned} \tag{3.11}$$

One gets

$$\frac{\partial \Psi}{\partial \mu} \Big|_1 = \frac{\Delta_1}{\Delta_0}, \quad \frac{\partial \Psi}{\partial \tau} \Big|_1 = -\frac{\Delta_2}{\Delta_0}, \quad \frac{\partial^2 \Psi}{\partial \mu^2} \Big|_1 = \frac{\Delta_3}{\Delta_0}, \quad \frac{\partial^2 \Psi}{\partial \tau^2} \Big|_1 = -\frac{\Delta_4}{\Delta_0}, \tag{3.12}$$

where Δ_i is the determinant of,

$$\begin{pmatrix}
\Psi_1 - \Psi_2 & \delta_{21}^\mu & \delta_{21}^\tau & (\delta_{21}^\mu)^2/2 & (\delta_{21}^\tau)^2/2 \\
\Psi_1 - \Psi_3 & \delta_{31}^\mu & \delta_{31}^\tau & (\delta_{31}^\mu)^2/2 & (\delta_{31}^\tau)^2/2 \\
\Psi_1 - \Psi_4 & \delta_{41}^\mu & \delta_{41}^\tau & (\delta_{41}^\mu)^2/2 & (\delta_{41}^\tau)^2/2 \\
\Psi_1 - \Psi_5 & \delta_{51}^\mu & \delta_{51}^\tau & (\delta_{51}^\mu)^2/2 & (\delta_{51}^\tau)^2/2
\end{pmatrix}, \tag{3.13}$$

with the $(i+1)^{\text{th}}$ column removed. Substituting these approximations for the differentials into Eq. (3.10), one obtains the second-order Taylor approximation to the point $\Psi(\mu_6, \tau_6)$, as required.

This system has been implemented for the vacuum case ($\mathcal{H}_\phi = 0$) for an initially Gaussian wave-packet along the μ -direction. As shown in Fig. 7, the initial data consist of two μ -rows of data, adjacent in the τ -direction and the data along the left-hand diagonal. One can also see from Fig. 7 that only data points within a similar diagonal on the right-hand side can be calculated. This results in the (μ, τ) being restricted to a triangle of base $\mu_{\max} - \mu_{\text{initial}}$ and

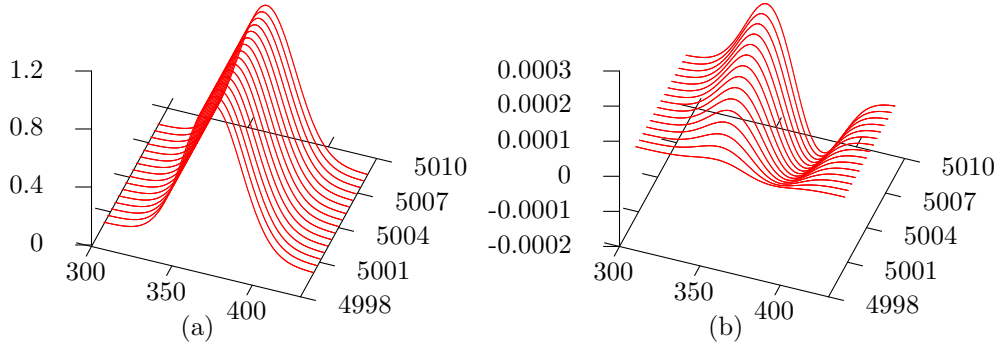


FIG. 8: The wave-function is calculated by iterating the difference equation using first-order Taylor expansion to evaluate the necessary data points at each site. The initial conditions are a Gaussian on $\tau_{\text{initial}} = 5000$, centred between $\mu_{\text{initial}} = 100$ and $\mu_{\text{max}} = 735$, of width $\sigma = 25$. The lattice refinement model used is $\delta_{\mu}(\mu, \tau) = \mu^{-1/2}$, $\delta_{\tau}(\mu, \tau) = \tau^{-1/2}$. Only the relevant section of the wave-function is plotted and to improve clarity, only every 20th- τ lattice point is shown. In (a) the propagation of the the wave-function is shown, whilst in (b) the value of the second-order terms is plotted. The second-order corrections are typically of the order of 10^{-2} % over this range.

height $\tau_{\text{max}} - \tau_{\text{initial}}$. Figure 8a shows a typical output using the first-order approximation evaluated for the lattice refinement model $\delta_{\mu}(\mu, \tau) = \mu^{-1/2}$, $\delta_{\tau}(\mu, \tau) = \tau^{-1/2}$, whilst Fig. 8b gives the second-order correction to this. It is clear that, at least for slowly varying wave-functions, the linear approximation is extremely accurate (higher-order corrections being $\approx 10^{-2}$ %).

IV. STABILITY OF THE SCHWARZSCHILD INTERIOR

In Ref. [5] a von Neumann stability analysis of the difference equation, Eq. (3.3), was performed for two lattice refinement models, and it was shown that in certain circumstances the system is only conditionally stable. In particular, it was found that for $\delta_{\mu}(\mu, \tau) = \mu_0 \mu^{-1}$ and $\delta_{\tau}(\mu, \tau) = \tau_0 \tau^{-1}$, the system is unstable for $\mu > 2\tau$.

We investigate this instability numerically and show that the stability condition is indeed correct. We do this by using the scheme described above to evaluate the wave-function, given two initial (consecutive) μ rows, that are empty apart from a small (10^{-6}) perturbation at a particular value of μ . The perturbation needs to be small to ensure we remain in the *pre-classical* regime. The system is then evaluated according to the the difference equation, Eq. (3.3), across different ranges of τ . Figure (9) shows a typical example of how the amplitude of the perturbation varies with τ .

By repeating this over a range of μ -positions for the perturbation, we are able to empirically confirm the stability condition $\mu < 2\tau$. We use this method to investigate how the lattice refinement model alters the stability properties of the system. In particular, we find that for $\delta_{\mu} = \mu^{-A}$ and $\delta_{\tau} = \tau^{-A}$, the stability condition ranges between $\mu < 4\tau$ for the $A = 0$ case (constant lattice) and $\mu < 1.58\tau$ for the case of $A = 2.0$. Figure 10 shows the cases in between. In all cases, the second-order correction terms are at least an order of magnitude lower than the wave-functions.

It is worth noting that for the constant lattice case, one does not have to perform any

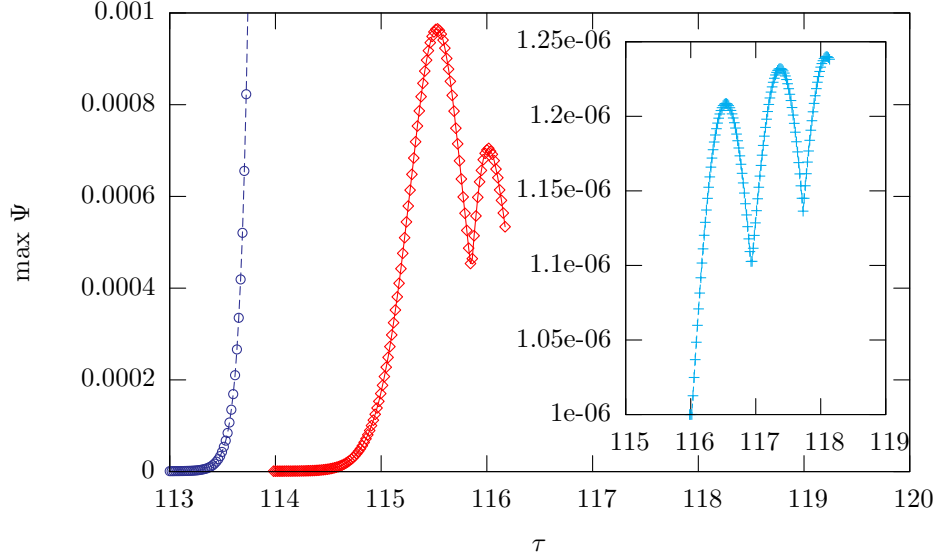


FIG. 9: A perturbation of $\Psi = 10^{-6}$ was put on an otherwise empty initial μ -row at $\mu = 230$, for the lattice refinement model $\delta_\mu(\mu, \tau) = \mu^{-1}$, $\delta_\tau(\mu, \tau) = \tau^{-1}$. The maximum amplitude of the resulting wave-function is plotted as a function of τ , for the initial perturbation set at $\tau = 113$, $\tau = 114$ and $\tau = 116$. Analytically, the region of stability is given for $\tau > \mu/2$, i.e., the amplitude of the perturbation grows exponentially for $\tau < 115$ and oscillates for $\tau > 115$. Here we confirm this numerically. Note the different scale on the graph starting within the stable region.

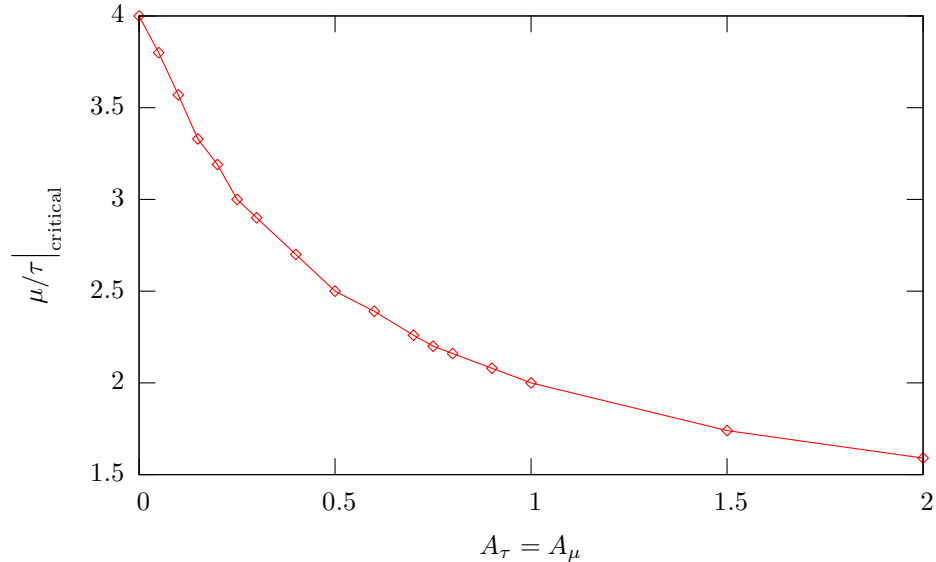


FIG. 10: For the lattice refinement models $\delta_\mu = \mu^{-A_\mu}$ and $\delta_\tau = \tau^{-A_\tau}$, the condition of stability has been found. Here we plot μ/τ along the critical line, i.e., the line in which the system is just becoming unstable, as a function of the parameter A .

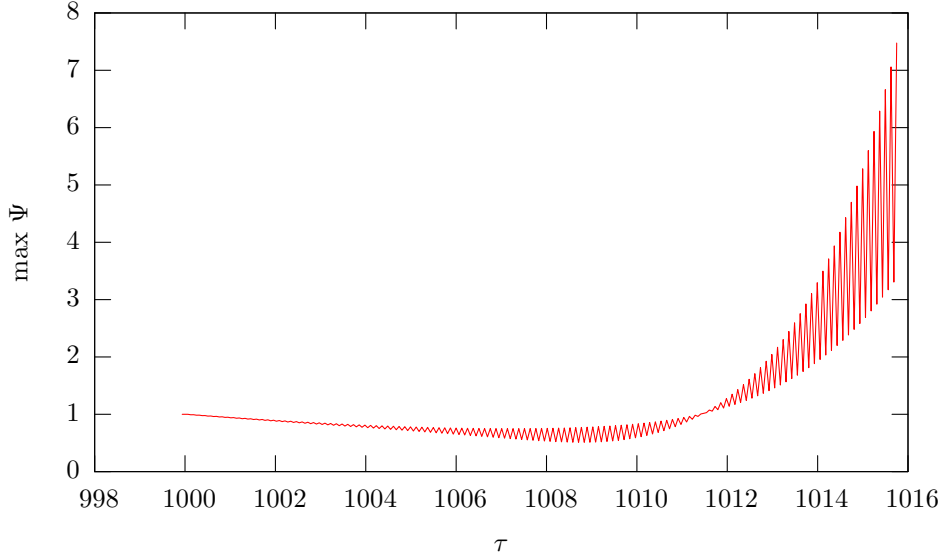


FIG. 11: The maximum amplitude for a Gaussian wave-packet centred on $\mu = 1060$ of width $\sigma = 5.25$, using the lattice refinement model $\delta_\mu = \mu_0\sqrt{\tau}\mu^{-1}$ and $\delta_\tau = \tau_0\tau^{-1/2}$. For small τ the solution does not vary significantly on scales of the order of the lattice size and hence the solution is stable, however as soon as the solution begins to vary this stability is lost.

interpolations to evaluate the wave-function. Thus, one does not require the wave-function to be *pre-classical* and large changes between successive lattice points are perfectly acceptable. However, such wave-functions clearly do not have a semi-classical limit². This is not true for the varying lattice cases, where for the interpolation to have a significant meaning, one must require that the wave-function be *pre-classical* (so that the derivatives in the Taylor expansion are small). We ensure that the stability condition holds by taking a small perturbation ($\approx 10^{-6}$). This is demonstrated well by the fact that for the case of $A = -1$, our results confirm the analytic considerations of Ref. [5].

In Ref. [5] a second lattice refinement model was shown to be unconditionally stable, under certain circumstances. Specifically, for $\delta_\mu(\mu, \tau) = \mu_0\sqrt{\tau}\mu^{-1}$ and $\delta_\tau(\mu, \tau) = \tau_0\tau^{-1/2}$, assuming the solutions do not change significantly on the scale of the step-sizes, the difference equation was found to be stable [5]. We find that this is indeed true, however as soon as the wave-functions fail to be *pre-classical*, i.e., as soon as there is a significant variation between lattice points (of the order of a few percent), they become unstable. In Fig. 11 we evaluate a Gaussian (centred on $\mu = 1060$ of width $\sigma = 5.25$) for this lattice refinement model. This solution is not entirely *pre-classical*, since there is a variation of $\approx 0.1\%$ between the wave-function evaluated on successive τ lattice points. This variation grows and when it reaches the order of a few percent the system becomes unstable. The rate at which small initial variations grow, and hence the rate at which the instability becomes apparent, depends on the μ - and τ -coordinates, growing faster for large μ and small τ .

Nevertheless, these instabilities do not represent any significant problem for loop quantum gravity approaches to black holes. It is already known that solutions must be *pre-classical* in

² When plotting these results, only values at the lattice points should be used, since the system is inherently discrete, however to guide the eye we have plotted the results with lines.

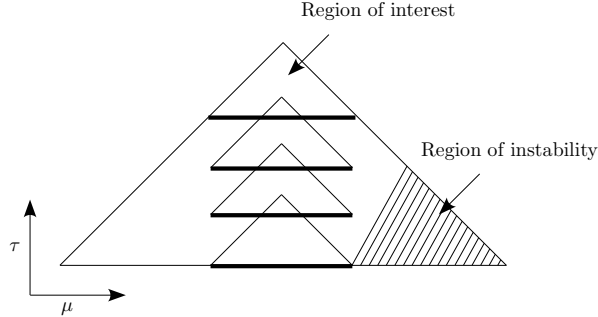


FIG. 12: The instability present in the difference equation occurs for large μ and small τ . If one is interested in reaching the value of the wave-function at large τ , one needs to have a large initial range of μ to have sufficient data. This can result in a portion of the domain being in the unstable region, which makes the code very sensitive to numerical inaccuracies. To avoid this, one can simply use a restricted μ -range and evaluate the wave-function as far as possible. This wave-function can then be used to create the initial conditions for a subsequent evaluation, provided the wave-function has not reached the edge of the lattice.

order to have a well-defined continuum limit (i.e., in order for $\lim_{\mu \rightarrow \infty, \tau \rightarrow \infty} \Psi_{\mu, \tau} = \Psi(\mu, \tau)$ to be valid). What is important is that this continuum limit is always stable, which is indeed the case for the $\delta_\mu = \mu_0 \sqrt{\tau} \mu^{-1}$, $\delta_\tau = \tau_0 \tau^{-1/2}$ lattice refinement model, but not for models of the form $\delta_\mu(\mu, \tau) = \mu_0 \mu^{-A}$, $\delta_\tau(\mu, \tau) = \tau_0 \tau^{-A}$.

The presence of these instabilities leads to difficulties in the numerical implementation of the method described above. In particular, if one wants to calculate the wave-function for large values of τ , then one needs to start with large range of μ , to ensure that enough initial data is known (see, Fig. 7). This can mean that the system is unstable at the large μ -side of the lattice, for small initial τ .

In practise, the value of the wave-function would usually be zero in this region, since one is typically interested in how an initial wave-packet evolves. Any non-zero component of the wave-packet in this unstable region would have met the right-hand diagonal edge of the lattice before the high τ -region of interest is reached. However rounding errors can result in a non-zero perturbation, which will grow exponentially due to the inherent instability of the difference equation. Such difficulties can be overcome, by evaluating the wave-function over a small region of τ . Since we now only require a smaller region of μ for this evaluation, the unstable region can be avoided. To reach the high τ -region of interest, the system can be re-set using the out-putted wave-function added to a larger range of μ , see Fig. (12). Alternatively, the additional initial data necessary to reach the large value of τ could be included at the evaluation of each μ -line, however this requires an additional three sets of τ -data, which effectively doubles the amount of initial data required.

V. PROPAGATION OF THE WAVE-FUNCTION

In the case of a constant lattice, an initially centred Gaussian will move to larger μ , as τ is increased (see, Fig. 13). [In terms of more usual coordinates, the angle Θ increases as the radius increases.] The reason for this can be seen simply by considering the original difference equation for the simple case of a lattice point on which $\Psi_{\mu, \tau} = 1$ and all other

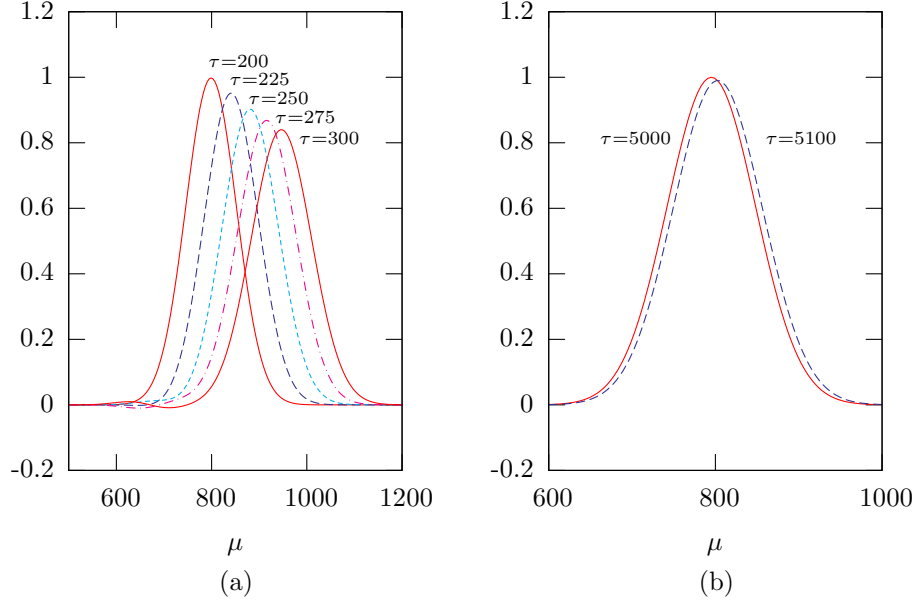


FIG. 13: (a) A Gaussian centred on $(\mu, \tau) = (800, 200)$ *twists* to larger values of μ as τ is increased. (b) As we move into the continuum limit this effect disappears. In this case the Gaussian is centred on $(\mu, \tau) = (800, 5000)$. Here the constant lattice case is shown however this effect persists when lattice refinement is modelled.

known Ψ -values are zero. Schematically, it is given by the lower hexagon in Fig. 14, centred around the non-zero wave-function $\Psi_{\mu, \tau}$. Then, Eq. (3.3) with $\gamma = 0$, implies

$$\Psi_{\mu+2\delta_\mu, \tau+2\delta_\tau} = 2C_0\mu/C_+ .$$

For $\tau \gg \delta_\tau$, this goes to zero. To see that this implies no motion of the wave-function, consider the next (upper) hexagon in Fig. 14, centred around the lattice point $\Psi_{\mu-2\delta_\mu, \tau+2\delta_\tau}$. If we ‘update’ the coordinates so that this central point is again called (μ, τ) , then, in these coordinates, only the lower right hand point in this (upper) hexagon is non-zero,

$$\Psi_{\mu+2\delta_\mu, \tau-2\delta_\tau} = 1 .$$

In this case, Eq. (3.3) gives

$$\Psi_{\mu+2\delta_\mu, \tau+2\delta_\tau} = C_-/C_+ ,$$

which tends to unity for $\tau \gg \delta_\tau$. Thus, we find that for large τ a value at one lattice point (μ, τ) , moves to one with the same μ -coordinate, $(\mu, \tau + 4\delta_\tau)$, i.e., there is no motion.

However, when we are in a region in which the lattice discreteness is important, this is no longer true, as $2C_0\mu/C_+ \neq 0$ and the value at one lattice point introduces a non-zero component to the value at a lattice point with larger μ coordinate, i.e., the wave-function moves to larger μ . This implies the existence of some induced rotation on the wave-function due to the underlying discreteness of the space-time.

If we include lattice refinement, then the same effect occurs. Once again, there is no motion for $\tau \gg \delta_\tau$ and in the case of lattice refinement this requirement is reached for lower τ , since δ_τ reduces as τ increases. Thus, we expect that the effect will disappear

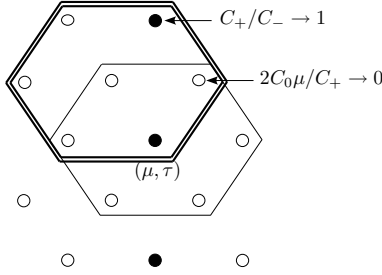


FIG. 14: By considering all the lattice points on the initial μ row except one being zero, the resulting wave-function can be calculated. When the discreteness cannot be ignored, there is a net *motion* towards larger values of μ (Θ). The lower hexagon shows the lattice points needed to evaluate the first step of the wave-function, whilst the upper hexagon highlights the points needed for the second step. The solid circles represent lattice points at which the wave-function is unity whilst at the open circles the wave-function is zero. From these it can be shown that the *twist* induced on the wave-function disappears on large-scales.

quicker than in the constant lattice case, because the lattice refinement brings us into the continuum limit faster. However once again, as the wave-function moves into a region in which the discreteness of the lattice is important, a motion will be induced.

VI. CONCLUSIONS

Here, we have developed a simple and intuitive prescription for evaluating two-dimensional wave-functions to a well-controlled level of accuracy, for arbitrary lattice refinement models. We focused on black-hole interiors, however the method clearly extends to anisotropic Bianchi models and other systems with anisotropic symmetries.

We have shown how the stability conditions on the Hamiltonian constraint can be investigated using this numerical method and extended the range of lattice refinement models for which the stability criterion are known.

We have also examined and explained the existence of a *twist* in the wave-functions, due to the underlying discreteness of the theory; a feature that warrants further study, particularly in relation to its effect in microscopic black holes.

VII. ACKNOWLEDGMENTS

This work is partially supported by the European Union through the Marie Curie REsearch and Training Network *Universeet* (MRTN-CT-2006-035863).

-
- [1] C. Rovelli, *Quantum Gravity* (Cambridge University Press, Cambridge, 2004).
 - [2] A. Ashtekar, M. Bojowald and J. Lewandowski, *Adv. Theor. Math. Phys.* **7** (2003) 233 [arXiv:gr-qc/0304074].
 - [3] M. Bojowald, *Class. Quant. Grav.* **19** (2002) 2717 [arXiv:gr-qc/0202077].

- [4] J. Rosen, J. H. Jung and G. Khanna, *Class. Quant. Grav.* **23** (2006) 7075 [arXiv:gr-qc/0607044].
- [5] M. Bojowald, D. Cartin and G. Khanna, *Phys. Rev. D* **76** (2007) 064018 [arXiv:0704.1137 [gr-qc]].
- [6] W. Nelson and M. Sakellariadou, *Phys. Rev. D* **76** (2007) 104003 [arXiv:0707.0588 [gr-qc]].
- [7] S. Sabharwal and G. Khanna, “Numerical solutions to lattice-refined models in loop quantum cosmology,” arXiv:0711.2086 [gr-qc].
- [8] A. Ashtekar, T. Pawłowski and P. Singh, *Phys. Rev. D* **74** (2006) 08400 [arXiv:gr-qc/0607039].
- [9] K. Vandersloot, *Phys. Rev. D* **71** (2005) 103506 [arXiv:gr-qc/0502082].
- [10] A. Ashtekar, J. C. Baez and K. Krasnov, *Adv. Theor. Math. Phys.* **4** (2000) 1 [arXiv:gr-qc/0005126].
- [11] A. Ashtekar and A. Corichi, *Class. Quant. Grav.* **20** (2003) 4473 [arXiv:gr-qc/0305082].
- [12] W. Nelson and M. Sakellariadou, *Phys. Rev. D* **76** (2007) 044015 [arXiv:0706.0179 [gr-qc]].
- [13] M. Bojowald, *Class. Quant. Grav.* **19** (2002) 5113 [arXiv:gr-qc/0206053].
- [14] A. Ashtekar and J. Lewandowski, *Class. Quant. Grav.* **21** (2004) R53 [arXiv:gr-qc/0404018].